IEEE Open Journal of
Power Electronics

Received 16 March 2022; revised 1 April 2022; accepted 6 April 2022. Date of publication 14 April 2022;
date of current version 2 May 2022. The review of this article was arranged by Associate Editor L. Hang.

Digital Object Identifier 10.1109/OJPEL.2022.3167548

Analysis of the Capacitor-Less D-STATCOM for Voltage Profile Improvement in Distribution Network With High PV Penetration

WESAM ROHOUMA [1] (Senior Member, IEEE), MORCOS METRY [2] (Member, IEEE), ROBERT S. BALOG [2] (Senior Member, IEEE), AAQIB AHMAD PEERZADA [3] (Student Member, IEEE), MIROSLAV M. BEGOVIC [3] (Fellow, IEEE), AND DAO ZHOU [4] (Senior Member, IEEE)

[1]Department of Electrical Engineering, the University of Doha for Science and Technology, 24449 Doha, Qatar
[2]Renewable Energy & Advanced Power Electronics Research Laboratory, Department of Electrical & Computer Engineering, Texas A&M University at Qatar, 23874 Doha, Qatar
[3]Department of Electrical & Computer Engineering, Texas A&M University, College Station, TX 77843 USA
[4]Department of Energy Technology, Aalborg University, 9220 Aalborg, Denmark

CORRESPONDING AUTHOR: WESAM ROHOUMA (e-mail: wesam.rohouma@ieee.org)

This work was supported by NPRP Grant 13S-0213-200357 from the Qatar National Research Fund (a member of Qatar Foundation). The statements made herein are solely the responsibility of the authors.

ABSTRACT Distributed Energy Resources (DERs) have disrupted the traditional electrical system. Grid-connected photovoltaic (PV) systems deliver electric energy closer to the consumer, shifting the paradigm from centralized to distributed generation. The impact of the stochastic PV output power gives rise to potentially rapid voltage fluctuations. Reactive power compensation is needed to regulate the voltage profile to meet the relevant standards. Traditional approaches like switched capacitors cannot provide reactive power that is continuously adjustable at short time scales. This paper examines an alternative distribution static synchronous compensator (D-STATCOM) based on a matrix converter (MC) for the low voltage distribution networks with high PV penetration. This technology can extend service life by using inductors for energy storage. The converter being studied provides ancillary services, including reactive power support; the impact on reliability, operational constraints, and electrical behavior is demonstrated. The contribution of this paper is a detailed analysis and impact study of the capacitor-less D-STATCOM in high PV penetration distribution networks. The significance of this paper is that it studies the behavior of the power electronics converter and its interaction with the power systems without assuming or neglecting details of either. Compensation effects and reliability comparisons between the proposed capacitorless D-STATCOM and the incumbent D-STATCOM technology are also studied in this paper.

INDEX TERMS D-STATCOM, voltage profile, reactive power compensation, model predictive control, matrix converter, grid integration, renewable energy sources, high PV penetration, reliability of power electronics.

NOMENCLATURE

T_S	Sampling time
k	The discrete sample time step
σ	Switching configuration number, $\sigma \in \{1, .., 27\}$
j	Phase $j \in \{A, B, C\}$
V_{oj}	The per-phase output voltage of the matrix converter
I_{oj}	The per-phase output current of the matrix converter
L_{MCj}	Per-phase output inductors
$R_{L_{MCj}}$	Per-phase parasitic resistance on output inductors
V_{Busj}	Per-phase input voltage of the filter
V_{ej}	Per-phase input filter output voltage (matrix converter input voltage)

I_{cj}	Per-phase input filter output current (matrix converter input current)
I_{ej}	The per-phase output current of the filter
R_{fj}	Per-phase parasitic resistance of the filter inductors
L_{fj}	Per-phase filter inductors
C_{fj}	Per-phase filter capacitors
I^*_{cj}	Reference input current in the MPC cost function
I^*_{oj}	Reference output current in the MPC cost function
g^{σ}	Objective cost function subject to switching state σ
$\lambda_1,\ \lambda_2$	MPC cost function weighting factors
M	Instantaneous transfer matrix for STATCOM
I_{Lj}	Per-phase load current
$S_{ij}(t)$	The switching function for i is an element of {A, B, C} and j is an element of {a, b, c} $S \epsilon \{01\}$
Z_n	Feeder impedance on the low voltage distribution network between bus-1 and bus-2 ($R_n + jX_n$)
ΔV_g	Voltage deviation between bus-1 and bus-2
$\alpha,\ \beta$	Parameters that define the exponential relationship of voltage with load active and reactive power
ψ^p_j	The rated peak active power of the jth PV system
P^p_i	Peak active load injection at i^{th} bus
r	Total number of PV systems deployed
N	Total number of buses in the distribution system
Q_{cb}	The reactive power exchanged between the converter and the bus where the converter is connected
$B,\ G$	Line susceptance and the conductance, respectively
V_{pcc}	The voltage at the point of common coupling (PCC)
V_{conv}	Converter voltage
$F_{conv}(t)$	Failure cumulative distribution function of a converter over time t in years
$F_{com}(t)$	Cumulative failure distribution function of a component
λ_Q, λ_D	Failure rate per year for the switch and diode, respectively
λ_E	The failure rate of energy storage device λ_C for capacitors and λ_L for inductors
$n_E\ n_Q\ n_D$	Number of components (energy devices, switches, and diodes, respectively) in converter topology
B_{10}	The time (years) by which the converter has a 10% probability of failure

I. INTRODUCTION

Recent International Renewable Energy Agency (IRENA) reports show that electrical power from photovoltaic (PV) systems increasingly costs less than electricity generated from fossil fuel sources [1]. Solar PV has over 500 GW of worldwide capacity installed [2]. As the PV penetration increases, various grid integration challenges arise. A consequence of the penetration of non-dispatchable PV DERs in the low-voltage network is more active power fed back to the grid. This reverse power flow in a distribution feeder causes several power quality issues, and one of these issues is the voltage rise in the feeder [3]–[5]. Another challenge with PV integration is the stochastic nature of the voltage fluctuation, impacted by dynamically changing weather patterns.

Power flows from generation to the end-user through the distribution network in a conventional power system. Accordingly, the load at the end of the low-voltage distribution network may experience poor voltage regulation due to the voltage drop in the distribution cables [6]. In the post-industrial digital economy, motors (linear loads) powering manufacturing have been replaced by computers (nonlinear loads) powering e-commerce. This phenomenon thus exacerbates grid integration challenges due to poor power quality (PQ) issues, resulting in further voltage drop.

Traditionally, various devices have been used to regulate the voltage at the distribution network, such as on-load tap changer transformers (OLTC) [7]–[11], volt/var control (VVC) with fixed capacitor banks (CBs) [12]–[14], or switched capacitors and inductors as in static var compensators (SVC) [15], [16]. Hybrid volt/var control combining OLTCs, CBs, and SVCs is typically utilized to provide var support [17]. These devices and technologies are not intended to mitigate such dynamic voltage fluctuation caused by PV penetration, as they can only inject a static or stepwise reactive power. The discrete levels of reactive power support do not allow for precise voltage control. The mechanical nature of OLTCs makes it harder to regulate the fast changes associated with intermittent nonscheduled PV generation. The result is a limited penetration capacity on the distribution feeder, endangering the grid's reliability and impacting the quality of the power delivered to the customers. Given the current and future projection of the distributed energy resources (DERs), the utilities of the future need fast-acting, solid-state-based solutions to provide dynamic and continuous adjustment of reactive power to achieve fast voltage regulation and power factor correction [18]. Fast-acting secondary side solutions must provide dynamic compensation at the source, co-located with the DER in the distribution system.

Many high-power smart PV inverters can provide ancillary services to the grid, and these inverters are in the 300kW range [19], [20]. PV inverters can provide reactive power support or curtail the active power to keep the network within operational constraints at the grid edge [21]–[24]. However, PV inverters are not utility-owned assets and are not directly controlled by the network operator.

A distribution static synchronous compensator (D-STATCOM) is a dynamic power electronics device that can provide flexible voltage regulation, power factor correction, and harmonics mitigation in the distribution network [18], [25]–[36]. Commercially available state-of-the-art D-STATCOM technologies are based on the voltage source converter (VSC) and rely on electrolytic capacitors (E-caps) for energy storage. E-caps are prone to numerous failures, particularly in warm locations [37]–[39]. E-caps were shown to cause 30% of power electronics failures [40]–[42].

TABLE 1. Comparing the Proposed Capacitorless D-STATCOM With Incumbent Technologies

	OLTC	CB	SVC	Hybrid VAR	Smart PV inverters	D-STATCOM	Capacitorless D-STATCOM
Dynamic reactive power compensation			✓		✓	✓	✓
Dynamic voltage regulation			✓		✓	✓	✓
Controlled by network operators	✓	✓	✓	✓		✓	✓
Long service life (avoids bulky E-caps)	✓						✓
Harmonic compensation					✓	✓	✓

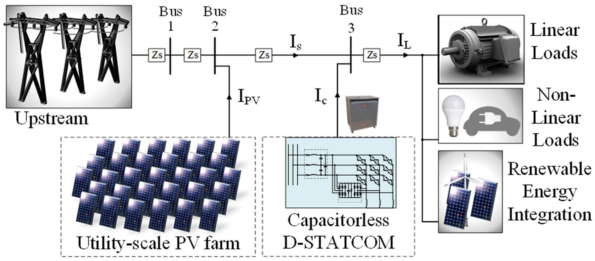

FIGURE 1. A one-line diagram of an example distribution system that illustrates the big picture concept. In addition to increasingly residential and commercial penetration of non-linear loads and renewable energy, this illustrative example considers a bus system with high utility-scale PV penetration. The impact of the capacitorless D-STATCOM voltage regulation is studied meticulously in this paper. Without loss of generality, the remainder of the distribution system to the sub-station is shows as "upstream".

A capacitorless D-STATCOM was developed and built based on the matrix converter (MC) and inductive energy storage, controlled using a finite control set model predictive control (MPC) is shown in [29], [43]–[46]. Compared to other incumbent technologies, the capacitorless D-STATCOM is capable of dynamic reactive power compensation, dynamic voltage regulation, and harmonic compensation while being controlled by the network operator, as shown in Table 1. In terms of impact, the capacitorless D-STATCOM has the same impact on the PV system as the incumbent VSC-based D-STATCOM technology. The only difference between the proposed capacitorless D-STATCOM and the incumbent D-STATCOM is inductors instead of capacitors for energy storage. Previous literature on the capacitorless D-STATCOM has focused on power electronics and controls [47]. The impact of the capacitorless D-STATCOM on the overall power system has not been as well studied.

This paper is built on the premise that the capacitorless D-STATCOM is proposed for the distribution network. This paper thus answers questions on (1) functional capabilities, (2) impact on the distribution network, (3) converter-level behavior, and (4) reliability of the proposed capacitorless D-STATCOM compared to other incumbent technologies (i.e., SVCs, VSC-based D-STATCOM, and OLTCs). The main contributions of this paper are:

- Impact study of capacitorless D-STATCOM on a distribution network with high PV permeability
- Circuit-level behavior comparison between capacitorless D-STATCOM and VSC-based D-STATCOM
- Reliability comparison between capacitorless D-STATCOM and VSC-based D-STATCOM

The significance of this paper is that it studies the behavior of the power electronics converter and its interaction with the power system without assuming or neglecting details of either. A study that combines both analyses has not been presented before.

This paper is arranged as follows: Section II introduces the power system study by detailing the impact of increased PV penetration on the distribution network. In the power system study of Section III, a complete OpenDSS simulation of the IEEE-34 bus distribution test system is used to illustrate the impact of the capacitorless D-STATCOM during high PV penetration. Section IV details the converter details and introduces the power electronics study. In the power electronics study of Section V, the electrical performance of the capacitorless D-STATCOM was demonstrated by a 7.5 kVA experimental prototype developed in the REAPER lab. Section VI is a discussion section that compares the compensation effects and reliability between the capacitorless D-STATCOM and state-of-the-art VSC-based D-STATCOM.

II. BIG-PICTURE IMPACT OF INCREASED PV PENETRATION IN THE DISTRIBUTION NETWORK

Consider the big-picture system one-line diagram of an example distribution system in Fig. 1. In addition to the increased residential and commercial penetration of nonlinear loads and renewable energy, this illustrative example considers a bus system with high utility-scale PV penetration. As the penetration levels of PV systems in distribution networks increase, a range of adverse power quality problems [48], [49] may appear, including:

- Reverse power flow: the increased proliferation of PV systems may offset local feeder loads and lead to reverse power flow that may affect overcurrent protection devices and the operation of voltage regulating equipment.
- Voltage rise: the voltage rise can be significant when large PVs are connected at the end of lightly loaded feeders. Voltage violation may happen and can trigger the overvoltage protection equipment.
- Voltage fluctuations: shading and cloud cover of PV systems can cause variations in output power, which can significantly impact feeder voltage.
- Interaction with available voltage regulating equipment: voltage rise and fluctuations may lead to the increased switching operation of voltage-controlled CBs, OLTC, and line VRs.
- Changes in feeder loading and electric losses: high PV permeability may reverse power flow, increasing power losses. Also, voltage rise may increase customer energy consumption (opposite the conservative voltage reduction method).

Voltage rise, voltage fluctuations, current, and voltage harmonics are significant problems in distribution feeders. The severity of these problems depends on PV penetration level, location of the PV, voltage control equipment such as voltage regulators (VRs), and CBs in the distribution feeder. These problems have a direct impact on network equipment. Voltage variations cause frequent operation of OLTCs, line VRs, and voltage-controlled CBs to control the feeder voltage, thus shortening the expected life cycle of these devices and increasing maintenance requirements [50], [51].

III. POWER SYSTEMS STUDY AND RESULTS

In this section, the proposed STATCOM is studied using a detailed OpenDSS simulation to understand its impact and behavior on the distribution network with high PV penetration. In Section III. A, simulation results that compare the voltage regulation impact of STATCOM and SVC technologies are presented. The STATCOM device is further studied within a distribution system outlined in Sections III.B and III.C. The simulation model and considerations are detailed in Sections III.D and III.E. The results of the power system simulations of the proposed STATCOM are presented in Section III.F.

A. STATCOM VS. SVC

SVCs are a practical alternative for voltage regulation and VAR compensation on the distribution network. Generally, SVCs are typical in medium voltage applications. The D-STATCOM in this paper is for low voltage application at the distribution feeder. In the later subsections, the capacitorless D-STATCOM is shown to precisely control the voltage and perform conservative voltage reduction to reduce losses, thus, improving the efficiency of the low voltage network.

This subsection compares a STATCOM device to an SVC device for voltage regulation impact through a simulation. For a fair comparison, both STATCOM and SVC have the same rating of 80 MVA. ABB has commercially marketed high VA rated STATCOM comparable to SVC scales [52], [53]. In this simulation, the IEEE-14 bus system is considered. The compensator is placed at node 7, congruent with [54]. A 200 MW PV farm is modeled on node-9 as was done in [55].

Consider the PV power profile shown in Fig. 3(a), with a typical power profile of a solar day. The left segment in Fig. 3 shows the PV profile's impact on the bus voltages at different segments of the IEEE-14 bus system, with a significant voltage variation. Using an 80 MVA static compensator at node-7 is shown to reduce the voltage variation. In this example, both SVC and STATCOM devices with the same ratings have the same voltage regulation impact on various buses on the bus system.

The STATCOM device has the same voltage regulation impact on the distribution network as the SVC. However, the STATCOM device performs more functions for the distribution network, such as harmonic compensation. The proposed capacitorless D-STATCOM does not rely on E-caps, unlike SVCs.

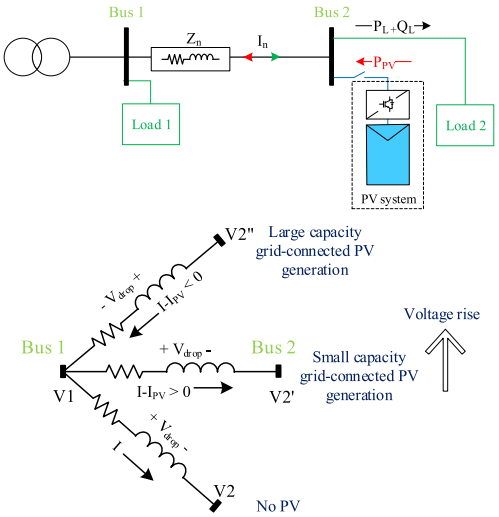

FIGURE 2. Low voltage distribution network with high PV penetration scenarios. V_2 is the base-case bus voltage without PV. The voltage at bus-2 increases to V_2' and V_2'' as more generation is added.

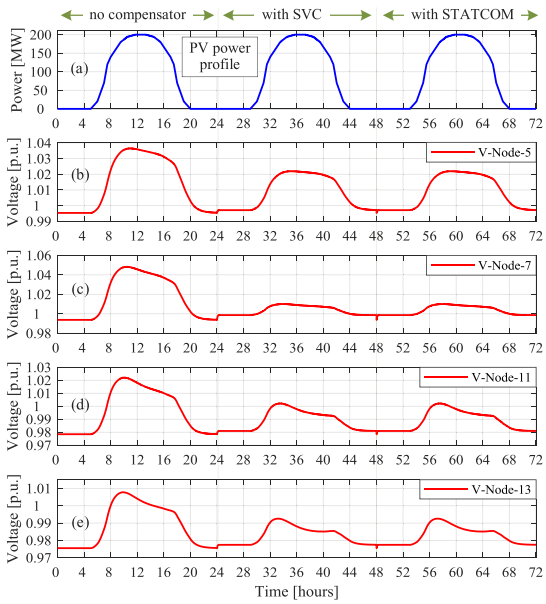

FIGURE 3. The voltage profile at different buses on an IEEE-14 bus system with high PV penetration of 200 MW at node 9. Without any compensator, the voltage change is significant. Using an 80 MVA static compensator at node 7 is shown to reduce the volage variation. In this example both SVC and STATCOM devices with the same ratings, have the same voltage regulation impact on various buses on the bus system.

B. DESCRIPTION OF A DISTRIBUTION TEST SYSTEM

Power flows bidirectionally with distributed PV penetration in low-voltage (LV) distribution networks, illustrated in Fig. 2, causing significant voltage profile disparity. The LV distribution networks have unique characteristics, such as dynamic loads and high resistance/reactance (R/X) ratio [56]. The voltage deviation ΔV_g between bus-1 and 2 along the feeder, due

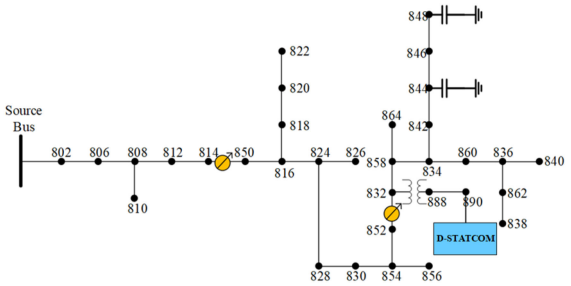

FIGURE 4. One-line diagram of distribution system with high PV penetration. The proposed D-STATCOM is shown shunt connected at bus 890 to provide reactive power compensation.

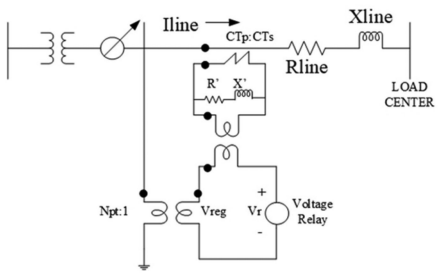

FIGURE 5. Line Drop Compensation Circuit.

to the current injection from bus-2, can be expressed as:

$$\Delta V_g = I_n Z_n \tag{1}$$

where Z_n is the feeder impedance $(R_n + jX_n)$. The bus voltage deviation at the point of connection V_g can be written as [56]:

$$\Delta V_g = \frac{R_n.P_g + X_n.Q_g}{|V_g|} + j\frac{X_n.P_g - R_n.Q_g}{|V_g|} \tag{2}$$

From (2), the bus voltage can be approximated [56]:

$$V_g \approx V_{g-1} + \frac{R_n.P_g + X_n.Q_g}{|V_g|} \tag{3}$$

According to (2) and (3), the voltage drop between the buses depends on the active power P_g, reactive power Q_g, and line impedance values. It can be noticed that without PV, the power flows in one direction from the distribution transformer to the load, and this causes voltage reduction at bus-2, as in Fig. 2. On the other hand, voltage rise occurs due to reverse power flow from the PV system. The rise of the voltage level depends on the associated reverse power flow and the line impedance between the bus and the closest voltage regulating devices. A utility-owned compensator could be connected at bus-2 to provide the required compensation to control the voltage profile and allow more distributed PV integration in LV distribution networks.

C. PARAMETERS OF THE IEEE-34 BUS SYSTEM

Consider the system-wide impact of high PV penetration on distribution systems by studying the model of the IEEE-34 bus system. The IEEE-34, shown in Fig. 4, is a 24.9 kV radial distribution network characterized by long lines and light loads. The circuit consists of a 2500 kVA, 69 kV/24.9 kV, Δ-Y substation transformer, two in-line three-phase VRs, an in-line 500 kVA, 24.9 kV/4.16 kV Δ-Y transformer at the start of the 832–890 lateral. The distribution system is also equipped with two three-phase fixed CBs with a combined rating of 750 kVAR. At bus 844, a 300 kVAR three-phase shunt capacitor bank is connected, while a larger 450 kVAR bank is connected to bus-848.

The load center for the first-in-line VR from the substation transformer (referred to as VR-1) is bus-814R, while

TABLE 2. Voltage Regulator (VR) Settings

Design Setting	VR-1(Phase A,B,C)	VR-2 (Phases A,B,C)
Voltage Level	122V	124V
Bandwidth	2V	2V
Time Delay	15 seconds	15 seconds
PT-Ratio	120	120
CT-Ratio	100	100
R	2.7 V	2.5 V
X	1.6 V	1.6 V
Connection	Wye-Wye	Wye-Wye
Location	Bus 814-814R	Bus 852-852R

the second voltage regulator (VR-2) controls the voltage of bus-852R. The VRs are based on the line drop compensation (LDC) circuit shown in Fig. 5 to maintain the voltage level. The LDC acts as a control circuit and models the voltage drop between the VRs and the load center to determine the tap position of the VR. The VRs' settings and the LDC circuit specifications are given in Table 2. Phase B and phase C settings are identical to phase A in both VRs. The setting for the bandwidth allows the load center voltage to be in the range of 121–123V for VR-1 and 123–125 V for VR-2.

A slightly higher voltage at the load center of VR-2 is to compensate for the significant voltage drop in the 832–890 lateral. The time delay precludes the VR from reacting to transient changes in the voltage or current. The VRs are equipped with a reversing switch which allows for a ±10% regulation range in 32 steps. On a 120V base, this translates to a 0.75 V change per step.

D. OPENDSS SIMULATION MODEL

In the OpenDSS simulation, the two three-phase VRs are modeled as six single-phase double-winding auto-transformers (with a VR control unit for each auto-transformer). Since the nominal feeder voltage is 24.9 kV, the rated voltage for the two windings of all single-phase autotransformers is 14.376 kV. The complete model of the distribution system consists of all single-phase and three-phase overhead lines, feeder VRs, customer loads, CBs, MV transformer, control circuits for the CBs, and VRs. The substation transformer is developed in OpenDSS [57].

The aggregate peak active load of the IEEE-34 system, as seen from the secondary of the substation transformer, is 2.04 MW. Based on the nominal values of the loads, the individual bus loads were divided into four categories, given

TABLE 3. Classification of Loads on IEEE 34 Distribution System

Load Class	Nominal kW Range
Small Dwelling (Studio Apartment)	$P_L \leq 3\ kW$
Large Dwelling (House with multiple bedrooms)	$3\ kW < P_L \leq 10\ kW$
Small Scale Commercial	$10\ kW < P_L \leq 25\ kW$
Medium Scale Commercial	$25\ kW < P_L \leq 100\ kW$
Large Scale Commercial	$100\ kW < P_L \leq 500\ kW$

in Table 3. Different load models were used: constant power loads - constant impedance loads - constant current loads - voltage-dependent loads were considered. Such load models represent the diversity of loads in MV/LV radial feeders and are consistent with the distribution test feeder IEEE specification. The dependency of the load active P_L and reactive Q_L powers on feeder voltages V is modeled as

$$\frac{P_L(V)}{P_{L0}} = \left(\frac{V}{V_0}\right)^{\alpha};\ \frac{Q_L(V)}{Q_{L0}} = \left(\frac{V}{V_0}\right)^{\beta} \tag{4}$$

where the parameters α and β define the exponential relationship. P_{L0} and Q_{L0} are the nominal power values, and V_0 is the base voltage.

E. SIMULATION CONSIDERATIONS

Consider the effect of distributed generation by studying a proportional-distributed grid-connected rooftop PV systems configuration. This configuration is most typical of distribution systems with a significant percentage of residential loads. The capacity of the PV system is rated based on the active load on the bus. Each grid-connected PV system is equipped with an inverter rated 10% higher than the peak capacity of the PV system.

Factoring in rooftop tilts and the direction in which the roofs of the houses in a typical residential neighborhood are facing, the tilt and azimuth angles of the rooftop PV systems are sampled from a uniform distribution. The optimal azimuth angle in the northern hemisphere is 180°, while the typical roof pitch in the USA is 4/12–9/12, which corresponds to pitch angles in the range of 18.43°–36.87°. Hence, a truncated uniform density with a mean of 180° for the azimuth angle and a uniform density with a mean of 27° to model the tilt angle of the grid-connected rooftop PV systems was selected. The transposition model of [58] is used to incorporate the information of the tilt and azimuth angle with the annual solar irradiance data of 1-minute temporal resolution to estimate the power output of the PV system. The PV penetration is given by

$$\%PV\ Penetration = \frac{\sum_{j=1}^{r} \psi_j^p}{\sum_{i=1}^{N} P_i^p} \times 100 \tag{5}$$

where, ψ_j^p is the rated peak active power of j^{th} PV system, P_i^p is the peak active load injection at i^{th} bus, r is the total number of PV systems deployed, and N is the total number of buses in the distribution system.

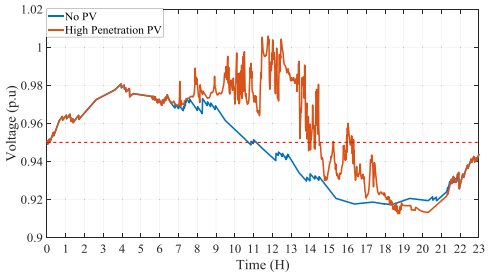

FIGURE 6. Voltage profile of bus 890 with and without high PV penetration. Increased penetration of PV can lead to a rise in the bus voltage during times of high solar irradiation.

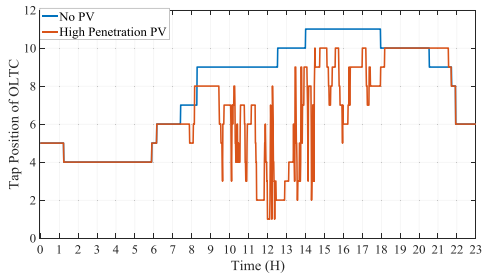

FIGURE 7. OLTC tap position with and without high PV penetration. Increasing the penetration of PV requires more frequency changes in the tap positions, increasing mechanical wear.

F. RESULTS: IMPACT OF HIGH PV PENETRATION

With the legacy voltage control framework (substation LTC, in-line VRs, and CBs) in operation, it is possible to control the slow variations in voltage due to load power injections. However, the stochastic nature of the PV generation results in highly variable voltages at the point of network connection. Legacy voltage control devices cannot mitigate such rapid excursions in bus voltages. The mechanical design of VRs and switched CBs renders them inadequate for regulating voltages at shorter time scales of minutes or seconds. Such highly fluctuating bus voltage profiles could stretch these devices to the limits of their operation and lead to the accelerated failure of VRs and switched CBs. The quasi-static time series (QSTS) simulations demonstrate the impact of continuous reactive power support for voltage regulation on a three-phase distribution feeder with VRs and switched CBs.

Consider the impact of high PV penetration on distribution system voltage with the full three-phase IEEE-34 bus distribution test feeder simulated in Open-DSS via a component object server (COMOS) and acts as a communication link between Open-DSS and MATLAB. Both steady-state and (QSTS) simulations are performed to assess the impact of high capacitive PV generation (90% penetration level). The effect of a highly variable voltage on OLTC operation is presented in Figs. 6 and 7.

As shown in Fig. 6, the bus voltage profile depicts a sustained increase in the PV systems voltage for the entire duration. When OLTCs or SCs encounter such a variable voltage

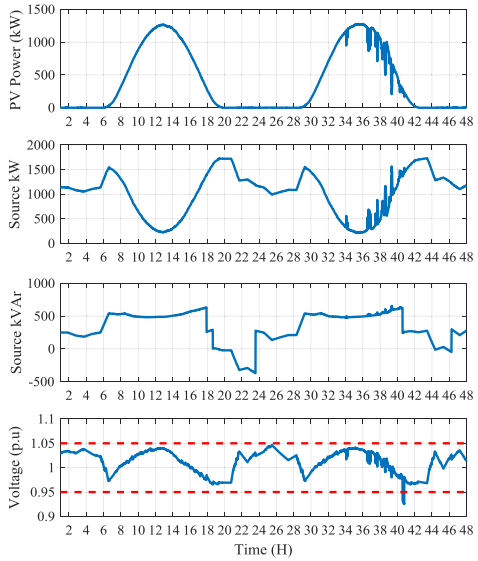

FIGURE 8. Results from QSTS simulation showing power flow and bus voltage without D-STATCOM.

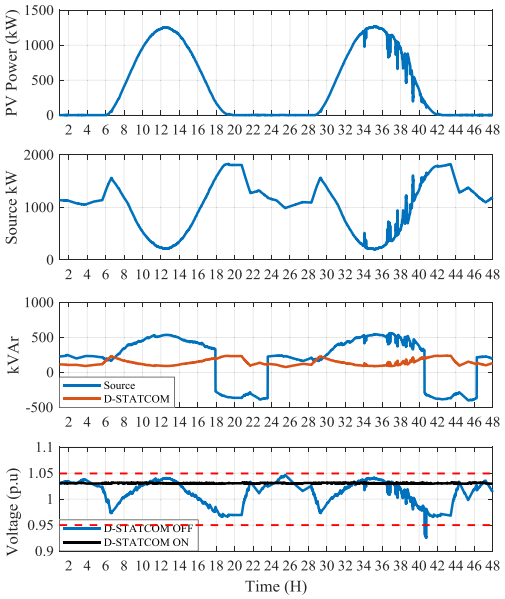

FIGURE 9. Results from QSTS simulation showing power flow and bus voltage with D-STATCOM.

on the secondary, their operational frequency significantly increases. The tap operation profile of an OLTC is shown in Fig. 7, corresponding to the voltage variation in Fig. 6. High PV penetration disturbs OLTCs operation, manifested as increased tap changing frequency to correct voltage variation. However, OLTCs cannot regulate the voltage under conditions of high penetration of intermittent nonscheduled generation. An uncontrollable voltage profile could further lead to load loss or a cascaded voltage collapse scenario. The penetration of PV systems has only increased over the last decade and will continue to rise further based on the current trends. Future utilities need fast-acting voltage controllers that can provide reactive power compensation at sub-minute time scales to mitigate the undesirable effects on system voltage caused by intermittent nonscheduled generation.

The proposed compensator can provide reactive power compensation and harmonic filtering at the LV network, the source of the power quality problem. Hence, eliminating the propagation of harmonics, voltage flicker, and voltage fluctuations upstream toward the source, i.e., distribution substation. To see the impact the proposed D-STATCOM would have on the tap-changing devices, a steady-state model of the D-STATCOM is developed in MATLAB and interfaced with OpenDSS via a COM interface. The steady-state voltage regulation model of the proposed D-STATCOM is based on the reactive power mismatch equations. The model uses a PID controller to minimize the reference and bus voltages mismatch. The mismatch equations are:

$$\begin{bmatrix} Q_{cb} - V_{pcc} I \sin\left(\theta_{V_{pcc}} - \theta_I\right) \\ Q_{cb} + \left|V_{pcc}\right|^2 B - \left|V'\right| G \sin\delta + \left|V'\right| B \cos\delta \end{bmatrix} = 0$$
$$\left|V'\right| = \left|V_{pcc}\right| \left|V_{conv}\right| \text{ and } \delta = \theta_{V_{pcc}} - \theta_{V_{conv}} \quad (6)$$

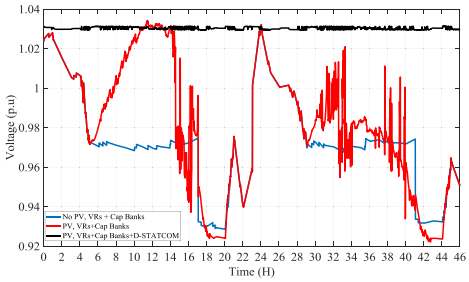

FIGURE 10. Impact of D-STATCOM on voltage profile of bus 890 without and with high PV penetration.

In (6), Q_{cb} is the reactive power exchanged between the converter and the bus where the converter is connected, B and G are the line susceptance and the conductance, respectively, V_{pcc} is the voltage at the point of common coupling (PCC) and V_{conv} is the converter voltage.

The interaction of the D-STATCOM with an OLTC is studied by connecting the two converters at bus-890. Bus-890 is on the secondary side of the VR-2, and bus-854 is on the primary side of the VR-2. The operation of the two converters is coordinated with the OLTC by setting the reference voltage of the two converters equal to the voltage set point of the VR. The VR changes taps whenever the measured load center voltage is outside the specified bandwidth for a duration that exceeds the time delay of the VR. The IEEE-34 feeder is subjected to QSTS simulations with a 90% PV penetration level and voltage of bus-890, and the corresponding tap profile of VR-2 is recorded.

Fig. 10 shows the voltage profile of bus-890 under different feeder conditions for the planning period of 48 hours, and

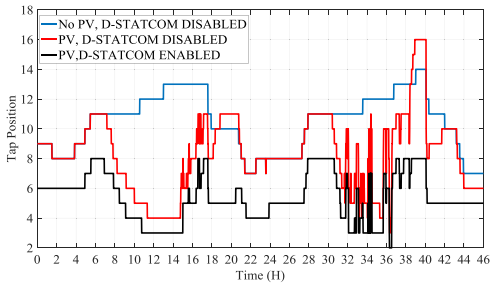

FIGURE 11. Impact of D-STATCOM on OLTC operation without and with high PV penetration over a 48-hour period. With the D-STATCOM in operation, the black curve shows the tap position of the VR as a function of time. The VR registers less operations with the D-STATCOM enabled than with D-STATCOM disabled. Over the course of a year, the D-STATCOM device has been shown to decrease VR tap operations by up to 95%.

TABLE 4. Cumulative Tap Operations

Device	Cumulative Tap Operations over a year		
	PV ON, D-STATCOM OFF	PV ON, D-STATCOM ON	% Decrease in Tap Operation
VR-1A	25,737	4,697	81.75%
VR-1B	10,561	516	95%
VR-1C	12,686	736	94.2%
VR-2A	24,161	11,407	52.7%
VR-2B	18,334	3,602	80.3%
VR-2C	18,811	4,606	75.5%

the tap profile of VR-2 is demonstrated in Fig. 11. The bus voltage is highly variable under high PV penetration and with D-STATCOM disabled and fluctuates rapidly. However, with the D-STATCOM enabled, the bus voltage is held nearly constant at 1.03 p.u. The voltage setting of the D-STATCOM is set equal to the setpoint of the nearest VR to ensure coordinated operation. With the D-STATCOM running in voltage regulation mode, OLTC registers fewer tap operations, corresponding to a decreased operational stress level on the VR. A direct consequence is a decrease in expected VR failures in high PV penetration conditions. Furthermore, with the D-STATCOM turned on, the VR consistently operates at lower tap positions, less likely to hit the maximum tap position. The results of the annual QSTS simulations of the cumulative number of tap operations of all the six phases of the two VRs are given in Table 4.

The continuously adjustable reactive power compensation capability of D-STATCOM could be further leveraged to provide several benefits such as minimizing power losses, improving power factor, and reducing harmonic losses. Thus optimize the converters' number, location, and voltage set points. Since the reactive output of PV inverters is limited by the amount of real power generated, the D-STATCOM offers superior performance in terms of capacity usage and control characteristics [29].

The injection of reactive power to regulate voltage alters the power flow and changes the overall feeder demand, as seen on the secondary of the substation transformer. The results shown in Figs. 8 and 9 were obtained by running daily QSTS simulations on the IEEE-34 feeder with and without a D-STATCOM at bus 890. The source power refers to the diversified demand (real and reactive) as seen on the secondary of the substation transformer.

IV. CONVERTER UNDER STUDY: CAPACITORLESS D-STATCOM

A D-STATCOM provides flexible voltage regulation, power factor correction, and harmonics mitigation in the distribution network [18], [25]–[36]. In electrical distribution systems, the motivations for providing reactive power support include minimization of feeder losses, flattening of feeder voltage profile, and improvement of substation power factor. In some cases, the dynamic dispatch of local volt-ampere reactive (VAR) compensation can also help extend the system's low-voltage ride-through capability, thereby mitigating the possibility of short-term voltage collapse. The reactive power support, which can be continuously adjusted, will help reduce the operational stress on the slow-acting mechanically switched devices, such as step-type VRs and switchable CBs. Such reactive power support source could either be run autonomously to achieve a set of predefined objectives or can be dispatched by the system operator.

Suppose the system operator wants to improve the power factor at a particular bus. The dispatch command will trigger the compensator to measure and supply the local reactive demand at the PCC. Whereas, if the objective is to reduce the operating frequency of the electromechanical devices on the feeder, the dispatch command could take the form of voltage regulation at the bus injection location. In the first scenario, the power quality compensator is expected to supply the local reactive power demand, thus eliminating the need to supply the reactive power from the source/substation. In the second scenario, the power quality compensator is expected to autonomously determine the required VARs to be produced or consumed to maintain the voltage within some determined limits. The current mechanical assets for voltage control operate on a slower time scale than the intermittency associated with the solar PV power injections. This mismatch renders the mechanically switched devices inadequate to correct the fast voltage variations.

In terms of impact and behavior, the capacitorless D-STATCOM is designed to perform the same functions as the incumbent VSC-based D-STATCOM technology. The only difference between the proposed capacitorless D-STATCOM and the VSC-based D-STATCOM is inductors instead of capacitors for energy storage. This section explains the control strategy that allows a matrix converter to rely on inductive energy storage to perform as a capacitorless D-STATCOM.

A. TOPOLOGY OF THE MATRIX CONVERTER

The MC-based capacitorless D-STATCOM shown in Fig. 12 is connected to the PCC through input filters, and the MC output is connected to inductive energy storage elements L_{MC}.

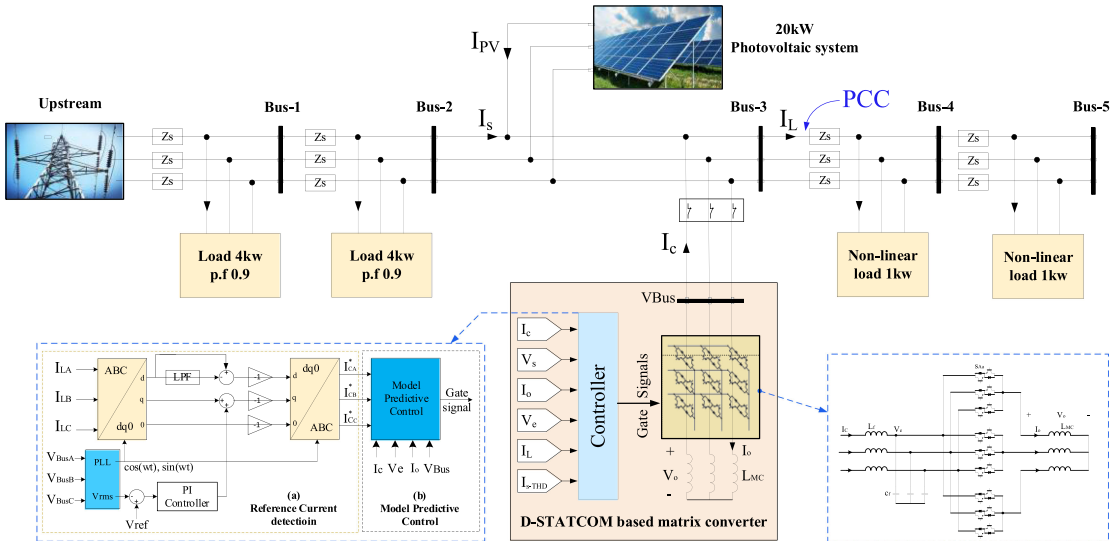

FIGURE 12. Detailed example system showing the capacitorless D-STATCOM device shunt connected at bus-3 Other buses in the vicinity are labeled as shown. Without loss of generality, the remainder of the distribution system to the sub-station is shows as "upstream".

The MC is a power electronics device that can perform direct ac/ac power conversion without E-caps. The MC topology comprises nine bi-directional switches realized by two anti-parallel IGBT-diode pairs for bidirectional flow.

B. THE ROLE OF CURRENT REVERSAL FOR INDUCTIVE STORAGE

The big-picture role of the MPC strategy is to achieve current phase inversion between the input and output currents. The energy storage on the MC absorbs the lagging current while the MC absorbs the leading current. In other words, the controller uses the measurements of the current harmonics on the distribution network to inject back the inverse harmonics, thus canceling out the harmonics on that bus. The result is a bus with lower harmonics and an improved voltage profile.

The relations between the input and output voltages and currents of the MC are in (7), (8), and (9). The switching function $S_{ij}(t)$ can be 0 or 1, where $i \epsilon \{A, B, C\}$ and $j \epsilon \{a, b, c\}$. Proper choice of S_{ij} achieves phase-reversal, thus making the inductive energy storage appear capacitive at the input of the MC [46], [59].

$$\begin{bmatrix} V_{oA} \\ V_{oB} \\ V_{oC} \end{bmatrix} = \begin{bmatrix} S_{Aa} & S_{Ab} & S_{Ac} \\ S_{Ba} & S_{Bb} & S_{Bc} \\ S_{Ca} & S_{Cb} & S_{Cc} \end{bmatrix} . \begin{bmatrix} V_{eA} \\ V_{eB} \\ V_{eC} \end{bmatrix} \tag{7}$$

$$\begin{bmatrix} I_{cA} \\ I_{cB} \\ I_{cC} \end{bmatrix} = \underbrace{\begin{bmatrix} S_{Aa} & S_{Ab} & S_{Ac} \\ S_{Ba} & S_{Bb} & S_{Bc} \\ S_{Ca} & S_{Cb} & S_{Cc} \end{bmatrix}}_{M} . \begin{bmatrix} I_{oA} \\ I_{oB} \\ I_{oC} \end{bmatrix} \tag{8}$$

$$S_{Aj} + S_{Bj} + S_{Cj} = 1 \; \forall \; j \epsilon \; \{A, B, C\} \tag{9}$$

where M is the instantaneous transfer matrix, V_{oj} a nd, I_{oj} are the output voltages and currents of the MC. V_{ej} and I_{cj} are the input voltages and currents of the MC (after the input filter).

The controller uses the voltage measurement at the PCC and the instantaneous three-phase load currents decomposed into real and reactive components (based on SRF [35], [60], [61]). The VR part compares the measured PCC voltage value with the required reference to generate the required reactive current for voltage regulation added to the reactive load current component, as in Fig. 12. The real component of the load current consists of a dc part representing the current's fundamental component and the ac part representing the harmonics. The harmonic component is extracted and then transformed back to the ABC reference frame as a reference current for the controller. More details on the controller are discussed in [46], [59].

C. MPC BASED CONTROL STRATEGY

The MPC-based controller relies on the converter relations to predict the switching configuration that minimizes the value of an error function to achieve the control objective. The predictive controller model relies on input and output currents predictions to perform the harmonic compensation, VAR compensation, and voltage regulation functions of the capacitorless D-STATCOM. The discrete-time estimate of the output current I_{oj}^{σ} at time sample $(k+1)$ is

$$I_{oj}^{\sigma}(k+1) = \left(1 - \frac{R_{L_{MCj}} T_s}{L_{MCj}}\right) I_{oj}(k) + \frac{T_s}{L_{MCj}} V_{oj}(k) \tag{10}$$

where σ is the switching configuration number, $\sigma \epsilon \{1, .., 27\}$, L_{MCj} and $R_{L_{MCj}}$ are the per-phase impedances of the energy storage devices.

TABLE 5. System Parameters for the Capacitorless D-STATCOM

Parameter	Value	Parameter	Value
Voltage, $V_{LL,RMS}$	415 V	Sampling time T_s	40µs
Line frequency	50Hz	Weight factor λ_1	2
Output chokes inductance L_{MC}	24mH	Weight factor λ_2	0.6
Input filter resistance R_f, L_f	1 Ω, 1mH	R_s	0.35 Ω
Input filter capacitor C_f	18 uF	L_s	1 mH
IGBT modules: SK60GM123		Voltage sensors: LEM LV-25P	
Clamp circuit for overvoltage protection		Current sensors: LEM LP-55	
Control platform: dSPACE Scalexio with 4 FPGA modules DS2655M1			
Upstream side: 12kVA three-phase grid simulator NHR-9410			
Downstream side: Electronic load from Cinergia			

The MC input current I_{oj}^{σ} of the converter can be written:

$$I_{cj}^{\sigma}(k+1) = -\frac{1}{L_f}V_{ej}(k) - \frac{R_f}{L_f}I_{cj}(k) + \frac{1}{L_f}V_{Busj}(k) \quad (11)$$

where L_f and R_f are the per-phase impedances of the input filter, V_{Busj} is the bus voltage (MC input voltage before the filter). The cost (error) function J is given as

$$g^{\sigma} = \lambda_1 \left| I_{cj}^{\sigma} - I_{cj}^{*} \right| + \lambda_2 \left| I_{oj}^{\sigma} - I_{oj}^{*} \right| \quad (12)$$

where I_{cj}^{*} and I_{oj}^{*} are the MC reference input and output currents. In this paper, λ_1 is given a higher priority with the ratio $\lambda_1/\lambda_2 = 3.5$.

V. POWER ELECTRONICS RESULTS

A. SIMULATION RESULTS

The dynamic compensation effects of the capacitorless D-STATCOM on the distribution network are verified through a MATLAB simulation. The system under study contains a three-phase source with series impedance to represent the upstream side of the distribution network, three-phase loads distributed through five buses, PV system with 20kW power. The proposed D-STATCOM device is connected at bus-3 as in Fig. 12 with parameters shown in Table 5.

In Fig. 13, the voltage profile across five buses with and without the D-STATCOM device being connected to bus-3. Without D-STATCOM, the voltage profile is changing as the PV system power varies during the day with poor voltage regulation at the buses located at the end of the feeder, where the voltage violates the limits of 228 (0.95 pu) and 252 (1.05 pu).

When the D-STATCOM device is connected to bus-3, it provides the necessary support to the network, and the voltage profile is improved across the distribution feeder. The three-dimensional view of the voltage profile across the five buses is plotted in Figs. 14 and 15. In Fig. 14, the voltage profile without D-STATCOM is presented changing as the power flow change in the network. At the same time, after adding the D-STATCOM device to bus-3, as in Fig. 15, it can be noted that the capacitorless D-STATCOM device has managed to flatten the voltage profile in the bus where it is connected and in the other buses in the feeder.

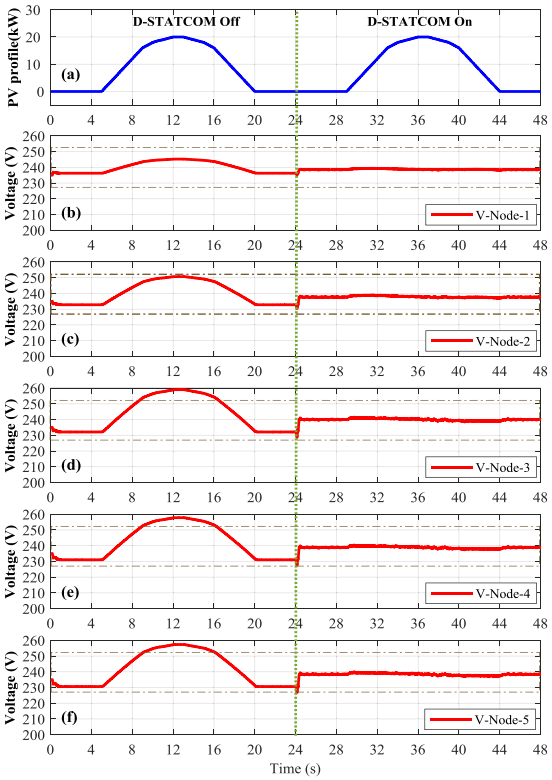

FIGURE 13. Voltage profile at different buses on the distribution feeder. D-STATCOM is connected at bus-3. The final 24-hours is without the capacitorless D-STATCOM compensator. The second 24-hours assumes identical system operation but adds the capacitorless D-STATCOM device.

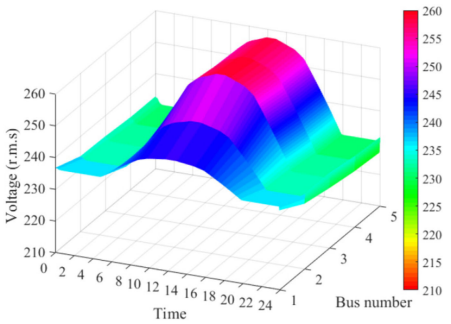

FIGURE 14. Feeder voltage profile of the system in Fig. 12 without D-STATCOM device.

B. EXPERIMENTAL RESULTS FOR THE CAPACITORLESS D-STATCOM

The proposed technology is validated experimentally using a 7.5 kVA matrix converter prototype with three-phase inductors on the output side for energy storage. As shown in Fig. 15, a reduced-scale experimental prototype is developed to validate the capability and effectiveness of the proposed capacitorless D-STATCOM in providing the necessary support to a low voltage distribution network. The details of the experimental prototype are shown in Table 5.

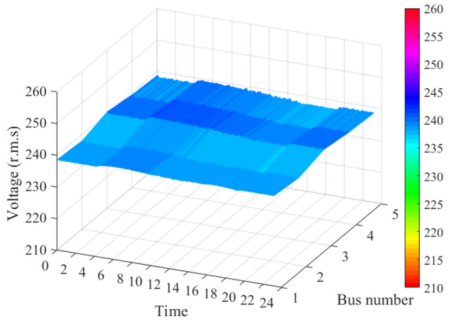

FIGURE 15. Feeder voltage profile of the system in Fig. 12 with D-STATCOM connected at bus-3.

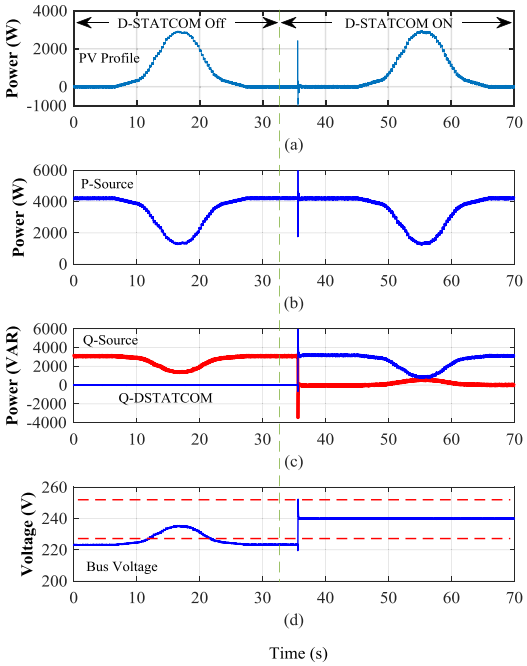

FIGURE 16. Experimental results showing PV system profile, upstream power, and D-STATCOM power and voltage profile at downstream.

Consider the impact of the D-STATOCM device on the downstream bus voltage profile in Fig. 16. Before connecting the D-STATCOM to the bus, the upstream provides the load with the active power of 4.2 kW and reactive power of 3 kVAR, while the D-STATCOM reactive power is zero. As the PV system injects 3 kW of active power to the downstream side, the active power changes are noted. The voltage profile downstream is fluctuating and violating the limits set by ANSI standards which can negatively impact the consumers connected to this bus. After the proposed D-STATCOM device is shunt connected to the downstream bus, dynamic reactive power injection to the grid enhances the voltage profile with good tracking to the 240 V reference.

Upstream voltage (V_s) and current (I_s) without D-STATCOM support is plotted in Fig. 18(a), the source current lags the voltage, and there is a phase shift between the voltage and the current. After the shunt-connected D-STATCOM device is enabled, it provides the necessary support with the source current leading the voltage due to the reverse reactive power injection to the source to compensate for the voltage drop in the series impedance. D-STATCOM reference and measured current of phase A are shown in Fig. 18(b); the controller was able to track the reference current. The upstream voltage distortion is still within limits recommended by standards, as shown in Fig. 18(b). Furthermore, the three-phase upstream current THD with the D-STATCOM device is shown in Fig. 18(b). The current THD in Fig. 18(b) is within limits specified by IEEE 519 [62], [63].

VI. DISCUSSIONS

Compared to other incumbent technologies, the capacitorless D-STATCOM is capable of dynamic reactive power compensation, dynamic voltage regulation, and harmonic compensation while being controlled by the network operator, as shown in Table 1. A summary of the impact of the capacitorless D-STATCOM on a distribution network with high permeability is outlined and discussed in Section VI.CA. The capacitorless D-STATCOM has the same impact on the PV system as the incumbent VSC-based D-STATCOM technology. The only difference between the proposed capacitorless D-STATCOM and the incumbent D-STATCOM is inductors instead of capacitors for energy storage. An impact and behavior comparison between the proposed capacitorless D-STATCOM and the incumbent D-STATCOM is discussed in Section VI.B with experimental results. A reliability comparison between the two technologies is further addressed in Section VI.C.

A. IMPACT OF THE CAPACITORLESS D-STATCOM ON A DISTRIBUTION NETWORK WITH HIGH PV PERMEABILITY

The main takeaways from the power system study presented in Section III:

- Capacitorless D-STATCOM can perform VAR compensation and voltage regulation in the distribution network.
- Dynamic harmonic compensation of the capacitorless D-STATCOM was shown to counteract PV variability in a distribution network with high PV permeability
- The capacitorless D-STATCOM provided dynamic support to the distribution network to allow more PV penetration.
- The capacitorless D-STATCOM could precisely control the voltage and perform conservative voltage reduction to reduce losses, thus, improving the efficiency of the low voltage network.
- A distribution network with high PV penetration and a capacitorless D-STATCOM has shown fewer tap changes in network mechanical OLTCs. Thus, increasing the service life of already existing distribution network equipment.

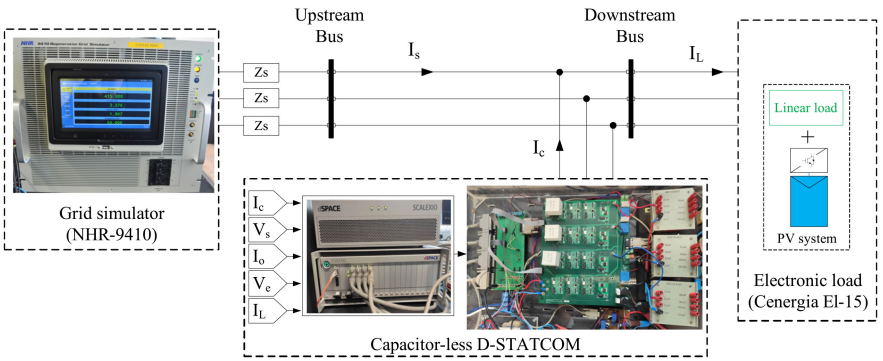

FIGURE 17. Hardware setup of a 7.5 kVA capacitor-less D-STATCOM system representing one bus in a radial destitution system. The upstream system is emulated by the grid simulator and the downstream loads are emulated by the electronic load.

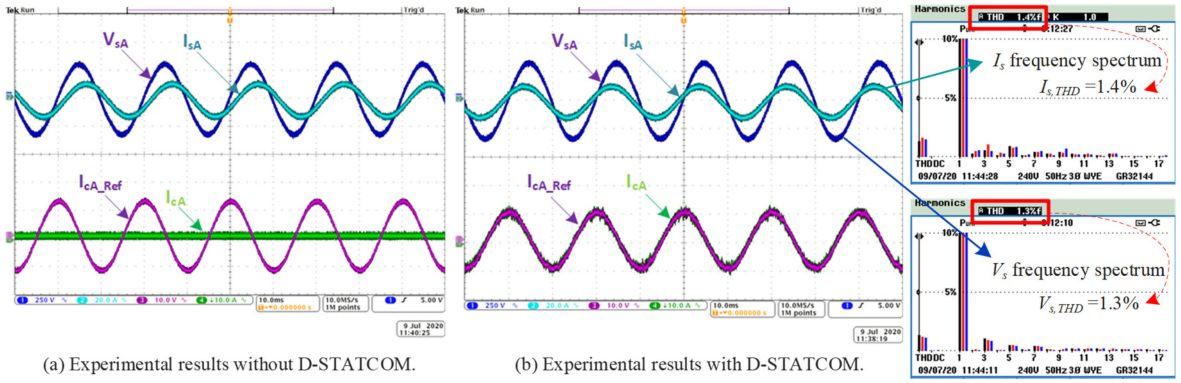

FIGURE 18. Experimental results showing upstream voltage and current (V_{sA},I_{sA}), and D-STATCOM reference and measured current (I_{cA_Ref},I_{cA}). (a) The waveforms without D-STATCOM. (b) The waveforms with proposed capacitorless D-STATCOM device connected. The compensation current I_{cA} tracks the reference current I_{cA_Ref}. The three-phase frequency spectra of the source voltages and currents (V_s and I_s) are plotted with THD of 1.3% and 1.4% for the voltage and current respectively.

TABLE 6. System Ratings VSC-Based D-STATCOM

Parameter	Value	Parameter	Value
Voltage, $V_{LL,RMS}$	415 V	Sampling time T_s	40µs
Line frequency	50Hz	Switching freq.	40 kHz
dc link E-caps	4 x 470 uF	Controller algorithm	PID
Input filter resistance R_f, L_f	1 Ω, 1mH	R_s	0.35 Ω
Input filter capacitor C_f	18 uF	L_s	1 mH
IGBT modules: SCT3080KLGC11		Control platform: dSPACE 1006	
Upstream side: 12kVA three-phase grid simulator NHR-9410			
Downstream side: Electronic load from Cinergia			

B. IMPACT AND BEHAVIOR COMPARISON BETWEEN INCUMBENT D-STATCOM AND CAPACITORLESS D-STATCOM

In terms of the compensation effect, the capacitorless D-STATCOM performs the same effect as the incumbent VSC-based D-STATCOM technology. In this subsection, comparative experimental results are presented. For the VSC-based D-STATCOM, a three-phase 7.5 kVA VSC motor drive manufactured by TARAZ technologies is used as the experimental setup with essential setup parameters in Table 6. For the sake of this subsection, the compensation effects were tested at $V_{s,RMS} = 200$ V. Testing at higher voltage, for the VSC-based D-STATCOM could be achieved using larger energy storage devices (more dc-link capacitors) and a pre-charging circuit. The experimental results of the comparative compensation effects of the different D-STATCOM technologies are shown in Fig. 19. The nonlinear load used in the testing (without D-STATCOM) has the waveforms shown in Fig. 19(a). Fig. 19(b) shows the results of the VSC-based D-STATCOM illustrating improved harmonic compensation. Fig. 19(c) shows the capacitorless D-STATCOM exhibiting similar impact and behavior as the incumbent D-STATCOM technology. While the waveforms and THD for the capacitorless D-STATCOM look slightly better than the VSC-based D-STATCOM, such effect is attributed to using a PID controller for the VSC-based D-STATCOM, with the possibility of improving the results with further tuning. The main takeaway is that both D-STATCOM technologies have the same compensation effects but rely on different energy storage devices (inductors vs. E-caps).

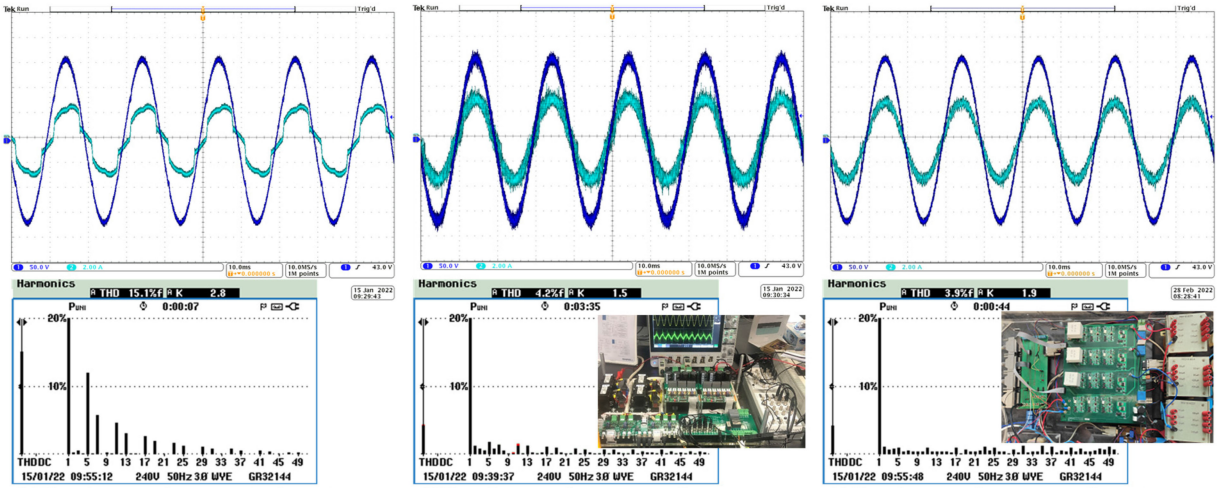

(a) Phase A source voltage, current and current harmonics without STATCOM connected.

(b) Phase A source voltage, current and current harmonics with VSC-based D-STATCOM connected.

(c) Phase A source voltage, current and current harmonics with capacitorless D-STATCOM connected.

FIGURE 19. Experimental compensation effect comparisons between traditional VSC-based D-STATCOM and proposed capacitorless D-STATCOM. The phase A source voltage, source current, and source current harmonics at 200 V with non-linear connected are presented. (a) Results without STATCOM connected showing the impact of the non-linear load on the distribution network. (b) Results with VSC-based D-STATCOM illustrating improved harmonic compensation. (c) Results with the capacitorless D-STATCOM illustrating similar impact and behavior as the incumbent D-STATCOM technology.

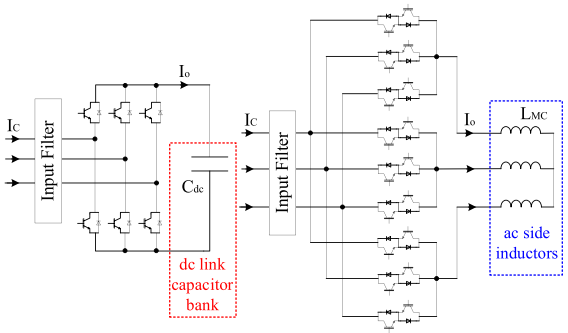

(a) VSC-based D-STATCOM (b) Capacitorless D-STATCOM

FIGURE 20. Circuit diagrams used in the reliability studies (a) incumbent VSC-based D-STATCOM, and (b) proposed capacitorless D-STATCOM based on matrix converter (MC).

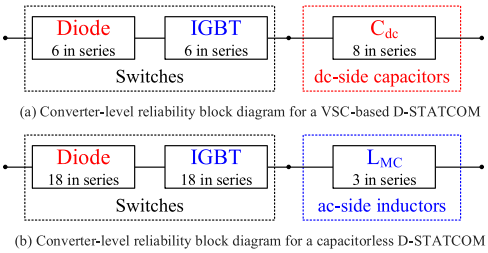

(a) Converter-level reliability block diagram for a VSC-based D-STATCOM

(b) Converter-level reliability block diagram for a capacitorless D-STATCOM

FIGURE 21. Converter-level reliability block diagram of the power switches, dc-side capacitors, and ac-side inductors for (a) incumbent VSC-based D-STATCOM, (b) proposed capacitorless D-STATCOM.

C. RELIABILITY COMPARISON BETWEEN INCUMBENT D-STATCOM AND CAPACITORLESS D-STATCOM

Considering the main application of the capacitorless D-STATCOM is in hot weather environments, mission profile data, based on Arizona USA ambient temperatures, is relevant to this analysis [64]. The failure rates are obtained from models presented in the military handbook MIL-HDBK-217F [65]. Since the handbook is old, the obtained component failure rates were adjusted to match other recent work relying on Monte-Carlo analyses [66]–[69]. From [66], the equivalent static value for mean junction temperature was found to be $T'_{jm} = 31.55°$ C for the mission profile for the state of Arizona and is thus used in this study.

Consider the circuit diagrams in Fig. 20 for the two 7.5 kVA D-STATCOM experimental prototypes form VI. B. In terms of characterizing the failure function, the converter-level reliability block diagrams of Fig. 21(a) and (b) show the components connected in series since a failure in any of the components results in total failure of the converter. The converter-level reliability diagram of the VSC-D-STATCOM (Fig. 21(a)) comprises six switches with six body diodes and a capacitor bank of eight capacitors. The connection of dc-link capacitors (series/parallel) is irrelevant in the reliability analysis since one capacitor failure tends to cascade to the other capacitors [70], [71]. Similarly, the converter-level reliability diagram for the capacitorless D-STATCOM (Fig. 21(b)) comprises eighteen switches with body diodes and three inductors.

Based on [65], the failure rates per year for the components of the D-STATCOM are $\lambda_D = 9.96 \times 10^{-6}$, $\lambda_Q = 1.89 \times 10^{-3}$, $\lambda_L = 2.64 \times 10^{-4}$, and $\lambda_C = 7.84 \times 10^{-3}$ for the diode, IGBT, inductor, and capacitor, respectively. The survival function of the exponential distribution can be used to model the component reliability function.

$$R_{com}(t) = e^{-\lambda t} \tag{13}$$

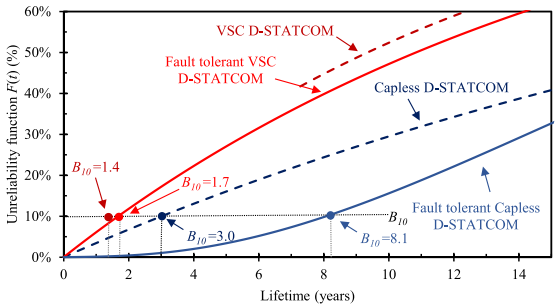

FIGURE 22. Unreliability functions for the VSC-based D-STATCOM and the capacitorless D-STATCOM installed in Arizona environmental conditions.

TABLE 7. Summary of Reliability Analysis Results

Technology	VSC[1]	Capless[2]	FT VSC[3]	FT Capless[4]
10-year reliability $R_{conv}(t=10)$	48%	71%	53%	84%
25-year reliability $R_{conv}(t=25)$	16%	42%	19%	36%
Converter-level lifetime - B_{10}	1.4 years	3.0 Years	1.7 years	8.1 years

[1]VSC-based D-STATCOM; [2]Capacitorless D-STATCOM; [3]Fault-tolerant (5-legged) VSC-based D-STATCOM; [4]Fault-tolerant (5-legged) Capacitorless D-STATCOM.

where t is the time in years. The converter failure function F_{conv} is calculated using

$$F_{conv}(t) = 1 - R_{conv}(t) = 1 - \prod R_{com}(t) \tag{14}$$

Thus, the converter failure function is

$$F_{conv}(t) = 1 - e^{-(n_D\lambda_D + n_Q\lambda_Q + n_E\lambda_E)t} \tag{15}$$

where λ_E is the failure rate per year of the energy storage device (λ_L for the inductor or λ_C for the capacitor), n_E, n_Q and n_d are the number of energy storage devices, IGBTs, and diodes, respectively.

The converter-level unreliability function curves for both converters based on Arizona environmental conditions are shown in Fig. 22. Based on the data considered in this analysis, Fig. 22 indicates that the VSC-based D-STATCOM is more prone to failure than the capacitorless D-STATCOM. The reliability function $R_{conv}(t) = 1 - F_{conv}(t)$. Based on the components' statistics the reliability of the incumbent VSC-based D-STATCOM is $R_{VSC,10} = 48\%$, and the reliability of the proposed capacitorless D-STATCOM is $R_{MC,10} = 71\%$ over a 10-year period. Summary of the reliability analysis results are shown in Table 7. The system-level B_{10} lifetimes, which correspond to the time by which the converter has 10% probability of failure, are shown in the same figure and summarized in Table 7. The B_{10} lifetime of the proposed capacitorless D-STATCOM is shown to be 53% longer than the incumbent VSC-based D-STATCOM.

A three-year B_{10} lifetime for the capacitorless D-STATCOM is still considered low, attributed mainly to the hot environment and the number of switches of the matrix converter. Previous work has considered a fault-tolerant capacitorless D-STATCOM [72], and the experimental prototype in Fig. 17 is a four-legged matrix converter. In this subsection, a five-legged D-STATCOM is analyzed. Regarding the reliability of a fault-tolerant converter, the fourth phase leg provides a contingency path to any of the three-phase legs. It is thus represented as four parallel reliability paths. The five legs of a fault-tolerant D-STATCOM is an example of an *m-out-of-n* (or m/n) parallel redundancy [73]. The reliability of the 5-legged converter with *3-out-of-5* redundancy can be represented as

$$R_{leg} = e^{-(n_D\lambda_D + n_Q\lambda_Q)t} \tag{16}$$

$$R_{sw} = 1 - \sum_{i=0}^{2} \binom{5}{i} \cdot R_{leg}^{i} \cdot \left(1 - R_{leg}\right)^{5-i} \tag{17}$$

$$R_{conv}(t) = R_{sw} \cdot R_E = R_{sw} \cdot e^{-n_E\lambda_E t} \tag{18}$$

The unreliability functions ($F_{conv} = 1 - R_{conv}$) of a fault-tolerant VSC-based D-STATCOM and a capacitorless D-STATCOM are plotted in Fig. 22. Considering a five-legged matrix converter in this study increases B_{10} lifetime of the capacitorless D-STATCOM to 8.1 years. A five-legged fault-tolerant VSC-based D-STATCOM has a B_{10} lifetime of 1.7 years. Thus, a fault-tolerant capacitorless D-STATCOM has a 79% longer life than a fault-tolerant VSC-based D-STATCOM. Results of the reliability comparisons and the B_{10} lifetimes are for a fault-tolerant capacitorless D-STATCOM compared to a fault-tolerant VSC-based D-STATCOM are summarized in Table 7. From this study, data corroborates the initial motivation for this research that the dc-link capacitors are the reliability bottleneck for the VSC-based D-STATCOM.

VII. CONCLUSION

This paper presented a detailed analysis and impact study of the capacitor-less D-STATCOM in high PV penetration distribution networks. This paper answered questions on (1) functional capabilities, (2) impact on the distribution network, (3) converter-level behavior, and (4) reliability of the proposed capacitorless D-STATCOM compared to other incumbent technologies (i.e., SVCs, VSC-based D-STATCOM, and OLTCs). The main contributions of this paper were:

- Impact study of capacitorless D-STATCOM on a distribution network with high PV permeability
- Impact and behavior comparison between capacitorless D-STATCOM and VSC-based D-STATCOM
- Reliability comparison between capacitorless D-STATCOM and VSC-based D-STATCOM

The significance of this paper is that it studies the behavior of the power electronics converter and its interaction with the power systems without assuming or neglecting details of either. In the power system study in this paper, a complete OpenDSS simulation of the IEEE 34 bus distribution test system was used to illustrate the impact of the capacitorless

D-STATCOM during high PV penetration. In the power electronics study, the converter-level behavior of the capacitorless D-STATCOM was demonstrated with a 7.5 kVA experimental prototype. The main findings of this paper:

- The capacitorless D-STATCOM provides dynamic support to the distribution network allowing more PV penetration.
- The capacitorless D-STATCOM could precisely control the voltage and perform conservative voltage reduction to reduce losses, thus, improving the efficiency of the low voltage network.
- A distribution network with high PV penetration and a capacitorless D-STATCOM has shown fewer tap changes in mechanical OLTCs. Thus, increasing the service life of already existing distribution network equipment.
- A reliability study of the D-STATCOM technologies has shown that dc-link capacitors are the reliability bottleneck of the incumbent VSC-based D-STATCOM.
- The capacitorless D-STATCOM has the same compensation effects as the VSC-based D-STATCOM without relying on E-caps.
- A fault-tolerant capacitorless D-STATCOM has a 79% longer life than a fault-tolerant VSC-based D-STATCOM.

ACKNOWLEDGMENT

The statements made herein are solely the responsibility of the authors.

REFERENCES

[1] H. Anuta, P. Ralon, M. Taylor, and F. L. Camera, *Renewable Power Generation Costs in 2019*. Abu Dhabi: International Renewable Energy Agency, Jun. 2020.

[2] IEA International Energy Agency, "*PVPS 2019: Snapshot of global PV markets*," Accessed: Jun. 2021. [Online]. Available: www.iea-pvps.org

[3] M. Thomson and D. G. Infield, "Impact of widespread photovoltaics generation on distribution systems," *IET Renewable Power Gener.,* vol. 1, no. 1, pp. 33–40, Mar. 2007.

[4] Y. Ueda, K. Kurokawa, T. Tanabe, K. Kitamura, and H. Sugihara, "Analysis results of output power loss due to the grid voltage rise in grid-connected photovoltaic power generation systems," *IEEE Trans. Ind. Electron.,* vol. 55, no. 7, pp. 2744–2751, Jun. 2008.

[5] R. Tonkoski, D. Turcotte, and T. H. El-Fouly, "Impact of high PV penetration on voltage profiles in residential neighborhoods," *IEEE Trans. Sustain. Energy,* vol. 3, no. 3, pp. 518–527, May 2012.

[6] F. Shahnia and A. Ghosh, "Coupling of neighbouring low voltage residential distribution feeders for voltage profile improvement using power electronics converters," *IET Gener., Transmiss. Distrib.,* vol. 10, no. 2, pp. 535–547, Feb. 2016.

[7] J. de Oliveira Quevedo *et al.*, "Analysis and design of an electronic on-load tap changer distribution transformer for automatic voltage regulation," *IEEE Trans. Ind. Electron.,* vol. 64, no. 1, pp. 883–894, Jul. 2016.

[8] C. R. Sarimuthu, V. K. Ramachandaramurthy, K. R. Agileswari, and H. Mokhlis, "A review on voltage control methods using on-load tap changer transformers for networks with renewable energy sources," *Renewable Sustain. Energy Rev.,* vol. 62, pp. 1154–1161, Sep. 2016.

[9] K. N. Bangash, M. E. A. Farrag, and A. H. Osman, "Smart control of on load tap changer deployed in low voltage distribution network," in *Proc. Int. Conf. Electric Power Energy Convers. Syst.*, 2015.

[10] T. Aziz and N. Ketjoy, "Enhancing PV penetration in LV networks using reactive power control and on load tap changer with existing transformers," *IEEE Access,* vol. 6, pp. 2683–2691, 2018.

[11] C. K. Gan, C. Y. Lau, K. A. Baharin, and D. Pudjianto, "Impact of the photovoltaic system variability on transformer tap changer operations in distribution networks," *CIRED - Open Access Proc. J.,* vol. 2017, no. 1, pp. 1818–1821, Jun. 2017.

[12] P. Kayal and C. K. Chanda, "Strategic approach for reinforcement of intermittent renewable energy sources and capacitor bank for sustainable electric power distribution system," *Int. J. Elect. Power Energy Syst.,* vol. 83, pp. 335–351, Dec. 2016.

[13] A. Ulinuha, M. A. S. Masoum, and S. M. Islam, "Optimal scheduling of LTC and shunt capacitors in large distorted distribution systems using evolutionary-based algorithms," *IEEE Trans. Power Del.*, vol. 23, no. 1, pp. 434–441, Dec. 2008.

[14] D. Q. Hung and Y. Mishra, "Voltage fluctuation mitigation: Fast allocation and daily local control of DSTATCOMs to increase solar energy harvest," *IET Renewable Power Gener.,* vol. 13, no. 14, pp. 2558–2568, Aug. 2019.

[15] Y. Ke, P. Huang, and T. Tseng, "Performance measurement of static var compensators in distribution system," in *Proc. Proc. SICE Annu. Conf.*, 2010.

[16] M. A. Talebi, A. Kazemi, A. Gholami, and M. Rajabi, "Optimal placement of static VAR compensators in distribution feeders for load balancing by genetic, algorithm," in *Proc. Int. Conf. Exhib. Electricity Distrib.*, 2005.

[17] W. Zhaoyu, C. Hao, W. Jianhui, and M. Begovic, "Inverter-Less hybrid voltage/var control for distribution circuits with photovoltaic generators," *IEEE Trans. Smart Grid,* vol. 5, no. 6, pp. 2718–2728, Sep. 2014.

[18] M. Begovic, A. Peerzada, S. Mohan, R. Balog, and W. Rohouma, "Impact of large distributed solar PV generation on distribution voltage control," in *Proc. 52nd Hawaii Int. Conf. System Sci.*, Maui, HI, USA, 2019.

[19] T. S. Marco, "Design of a 1MVA grid-tied photovoltaic plant in bugasong (Visayan islands-Philippines)," in *Industrial Technologies Engineering, Engineering Projects Department*, Spain: Polytechnic Univ. of Valencia Valencia, 2018. [Online]. Available: http://hdl.handle.net/10251/106802

[20] A. B. B. Group, "ABB central inverters PVS800 100 to 500kW." Accessed: May 2020, [Online]. Available: https://new.abb.com/docs/librariesprovider22/technical-documentation/pvs800-central-inverters-flyer.pdf?sfvrsn=2

[21] A. M. Howlader, S. Sadoyama, L. R. Roose, and S. Sepasi, "Distributed voltage regulation using Volt-Var controls of a smart PV inverter in a smart grid: An experimental study," *Renewable Energy,* vol. 127, pp. 145–157, Nov. 2018.

[22] P. Jahangiri and D. C. Aliprantis, "Distributed Volt/var control by PV inverters," *IEEE Trans. Power Syst.,* vol. 28, no. 3, pp. 3429–3439, Apr. 2013.

[23] K. A. Alboaouh and S. Mohagheghi, "Impact of rooftop photovoltaics on the distribution system," *J. Renewable Energy,* vol. 2020, pp. 1–23, Jan. 2020.

[24] A. Safayet, P. Fajri, and I. Husain, "Reactive power management for overvoltage prevention at high PV penetration in a low-voltage distribution system," *IEEE Trans. Ind. Appl.,* vol. 53, no. 6, pp. 5786–5794, Aug. 2017.

[25] N. K. Roy, H. R. Pota, and M. J. Hossain, "Reactive power management of distribution networks with wind generation for improving voltage stability," *Renewable Energy,* vol. 58, pp. 85–94, Oct. 2013.

[26] A. R. Gupta and A. Kumar, "Impact of various load models on D-STATCOM allocation in DNO operated distribution network," *Procedia Comput. Sci.,* vol. 125, pp. 862–870, Dec. 2018.

[27] B. Singh and J. Solanki, "A comparison of control algorithms for DSTATCOM," *IEEE Trans. Ind. Electron.,* vol. 56, no. 7, pp. 2738–2745, Apr. 2009.

[28] B. Singh, P. Jayaprakash, and D. P. Kothari, "A T-connected transformer and three-leg VSC based DSTATCOM for power quality improvement," *IEEE Trans. Power Electron.,* vol. 23, no. 6, pp. 2710–2718, Dec. 2008.

[29] W. Rohouma, R. S. Balog, A. A. Peerzada, and M. M. Begovic, "D-STATCOM for harmonic mitigation in low voltage distribution network with high penetration of nonlinear loads," *Renewable Energy,* vol. 145, pp. 1449–1464, Jan. 2020.

[30] R. Yan, B. Marais, and T. K. Saha, "*Impacts of Residential Photovoltaic Power Fluctuation On On-Load Tap Changer Operation and a Solution Using DSTATCOM*," ELSEVIER: Electric Power Systems Research, vol. 111, pp. 185–193, Jun. 2014.

[31] S. Srikanthan and M. K. Mishra, "DC capacitor voltage equalization in neutral clamped inverters for DSTATCOM application," *IEEE Trans. Ind. Electron.,* vol. 57, no. 8, pp. 2768–2775, May 2010.

[32] B. Singh, P. Jayaprakash, D. P. Kothari, A. Chandra, and K. A. Haddad, "Comprehensive study of DSTATCOM configurations," *IEEE Trans. Ind. Inform.,* vol. 10, no. 2, pp. 854–870, Mar. 2014.

[33] C. Kumar and M. K. Mishra, "A voltage-controlled DSTATCOM for power-quality improvement," *IEEE Trans. Power Del.,* vol. 29, no. 3, pp. 1499–1507, Apr. 2014.

[34] D. Q. Hung, Y. Mishra, and G. Walker, "Reducing voltage fluctuations using DSTATCOMs and reactive power of PV inverters in a medium voltage distribution system," *J. Eng.,* vol. 2019, pp. 5274–5279, Aug. 2019.

[35] F. Shahnia, S. Rajakaruna, and A. Ghosh, *Static Compensators (STATCOMs) in Power Systems*. Springer, 2015.

[36] C. Y. Reddy, V. Krishnakanth, R. Sanjay, V. N. V. Krishna, and R. Jayabarathi, "Laboratory implementation of automatic voltage regulator," in *Proc. Biennial Int. Conf. Power Energy Syst.: Towards Sustain. Energy*, 2016.

[37] H. Keyhani, M. Johnson, and H. A. Toliyat, "A soft-switched highly reliable grid-tied inverter for PV applications," in *Proc. IEEE Appl. Power Electron. Conf. Expo.*, Fort Worth, TX, USA, 2014, pp. 1725–1732.

[38] S. Harb and R. S. Balog, "Reliability of candidate photovoltaic module-integrated-inverter (PV-MII) topologies-A usage model approach," *IEEE Trans. Power Electron.,* vol. 28, no. 6, pp. 3019–3027, Oct. 2013.

[39] C. Lachkar *et al.*, "Failure analysis of aluminum electrolytic capacitors based on electrical and physicochemical characterizations," in *Proc. Int. Rel. Phys. Symp.*, 2017.

[40] T. Orłowska-Kowalska, F. Blaabjerg, and J. Rodríguez, *Advanced and Intelligent Control in Power Electronics and Drives*. Springer, 2014.

[41] S. Yang, A. Bryant, P. Mawby, D. Xiang, L. Ran, and P. Tavner, "An industry-based survey of reliability in power electronic converters," *IEEE Trans. Ind. Appl.,* vol. 47, no. 3, pp. 1441–1451, Mar. 2011.

[42] L. F. Costa and M. Liserre, "Failure analysis of the dc-dc converter: A comprehensive survey of faults and solutions for improving reliability," *IEEE Power Electron. Mag.,* vol. 5, no. 4, pp. 42–51, Dec. 2018.

[43] W. Rohouma, R. S. Balog, A. A. Peerzada, and M. M. Begovic, "Reactive power compensation of time-varying load using Capacitor-less D-STATCOM," in *Proc. Int. Conf. Power Electron.-ECCE Asia*, Busan, South Korea, 2019.

[44] W. Rohouma, R. S. Balog, A. A. Peerzada, and M. M. Begovic, "Development of a Capacitor-less D-STATCOM for power quality improvement in low voltage network," in *Proc. IEEE Int. Conf. Compat., Power Electron. Power Eng.*, Sonderborg, Denmark, 2019, pp. 1–5.

[45] W. Rohouma, R. S. Balog, A. A. Peerzada, and M. M. Begovic, "D-STATCOM for a distribution network with distributed PV generation," in *Proc. Int. Conf. Photovoltaic Sci. Technol.*, 2018.

[46] W. Rohouma, R. S. Balog, A. A. Peerzada, and M. M. Begovic, "Capacitor-less D-STATCOM for reactive power compensation," in *Proc. IEEE 12th Int. Conf. Compat., Power Electron. Power Eng.*, Doha, Qatar, 2018, pp. 1–6.

[47] W. Rohouma, M. Metry, R. S. Balog, A. A. Peerzada, and M. M. Begovic, "Adaptive model predictive controller to reduce switching losses for a capacitor-less D-STATCOM," *IEEE Open J. Power Electron.,* vol. 1, pp. 300–311, 2020.

[48] A. Anzalchi, A. Sundararajan, A. Moghadasi, and A. Sarwat, "High-Penetration grid-tied photovoltaics: Analysis of power quality and feeder voltage profile," *IEEE Ind. Appl. Mag.,* vol. 25, no. 5, pp. 83–94, Jul. 2019.

[49] M. Karimi, H. Mokhlis, K. Naidu, S. Uddin, and A. H. A. Bakar, "Photovoltaic penetration issues and impacts in distribution network – a review," *Renewable Sustain. Energy Rev.,* vol. 53, pp. 594–605, Jan. 2016.

[50] F. Katiraei and J. R. Agüero, "Solar PV integration challenges," *IEEE Power Energy Mag.,* vol. 9, no. 3, pp. 62–71, Apr. 2011.

[51] J. R. Agüero and S. J. Steffel, "Integration challenges of photovoltaic distributed generation on power distribution systems," in *Proc. IEEE Power Energy Soc. Gen. Meeting*, 2011, pp. 1–6.

[52] T. Larsson, R. Grunbaum, and B. Ratering-Schnitzler, "SVC light: A utility's aid to restructuring its grid," in *Proc. IEEE Power Eng. Soc. Winter Meeting. Conf. Proc. (Cat. No.00CH37077)*, Singapore, 2000, vol. 4, pp. 2577–2581.

[53] M. Noroozian, A. N. Petersson, B. Thorvaldson, B. A. Nilsson, and C. W. Taylor, "Benefits of SVC and STATCOM for electric utility application," in *Proc. IEEE PES Transmiss. Distrib. Conf. Expo. (IEEE Cat. No.03CH37495)*, Dallas, TX, USA, 2003, vol. 3, pp. 1192–1199.

[54] S. Gupta, S. Garg, V. Babbar, S. Saha, and N. Nagarwal, "Modeling and performance investigation of PV integrated IEEE 14 bus test system," in *Proc. Int. Conf. Comput., Power Commun. Technol.*, Greater Noida, India, 2018, pp. 275–279.

[55] I. Moufid, H. El Markhi, H. Moussaoui, and L. Tijani, "Best Place STATCOM IEEE 14 Bus System to Improve Voltage Profile Using Neplan Softw.," vol. 681, 2021, pp. 513–521.

[56] J. Hu, Z. Li, J. Zhu, and J. M. Guerrero, "Voltage stabilization: A critical step toward high photovoltaic penetration," *IEEE Ind. Electron. Mag.,* vol. 13, no. 2, pp. 17–30, Jun. 2019.

[57] R. C. Dugan, "Reference guide: The open distribution system simulator (OpenDSS)." Electric Power Research Institute, Accessed: Feb. 2020, [Online]. Available: https://spinengenharia.com.br/wp-content/uploads/2019/01/OpenDSSManual.pdf

[58] C. A. Gueymard, "From global horizontal to global tilted irradiance: How accurate are solar energy engineering predictions in practice?," in *Proc. Sol. Conf.*, San Diego, CA, USA, 2008.

[59] M. B. Shadmand, M. Mosa, R. S. Balog, and H. Abu-Rub, "Model predictive control of a capacitorless matrix converter-based STATCOM," *IEEE J. Emerg. Sel. Topics Power Electron.,* vol. 5, no. 2, pp. 796–808, Jun. 2017.

[60] S. Bhattacharya and D. Divan, "Synchronous frame based controller implementation for a hybrid series active filter system," in *Proc. IAS Annu. Meeting, Ind. Appl. Conf.*, 1995.

[61] B. Singh and V. Verma, "Selective compensation of power-quality problems through active power filter by current decomposition," *IEEE Trans. Power Del.,* vol. 23, no. 2, pp. 792–799, Mar. 2008.

[62] I. W. Group, "519-2014 - IEEE Recommended practice and requirements for harmonic control in electric power systems," *IEEE Std 519-2014 (Revision of IEEE Std 519-*1992), Standard pp. 1–29, Jun. 2014.

[63] Voltage Disturbances, Standard EN 50160, Wroclaw Univ. of Technology, Jul. 2004.

[64] A. Andreas and S. Wilcox. *Observed Atmospheric and Solar Information System (OASIS) - SOLRMAP University of Arizona: 2018 Data*, doi: 10.5439/1052226.

[65] *Military Handbook: Reliability Prediction of Electronic Equipment*, Standard MIL-HDBK-217F Dec. 1991.

[66] A. Sangwongwanich, Y. Yang, D. Sera, and F. Blaabjerg, "Lifetime evaluation of grid-connected PV inverters considering panel degradation rates and installation sites," *IEEE Trans. Power Electron.,* vol. 33, no. 2, pp. 1225–1236, Feb. 2018.

[67] K. Ma, H. Wang, and F. Blaabjerg, "New approaches to reliability assessment: Using physics-of-failure for prediction and design in power electronics systems," *IEEE Power Electron. Mag.,* vol. 3, no. 4, pp. 28–41, Dec. 2016.

[68] D. Zhou and F. Blaabjerg, "Converter-Level reliability of wind turbine with low sample rate mission profile," *IEEE Trans. Ind. Appl.,* vol. 56, no. 3, pp. 2938–2944, May/Jun. 2020.

[69] H. Wang *et al.*, "Transitioning to Physics-of-Failure as a reliability driver in power electronics," *IEEE J. Emerg. Sel. Topics Power Electron.,* vol. 2, no. 1, pp. 97–114, Mar. 2014.

[70] D. Zhou, Y. Song, Y. Liu, and F. Blaabjerg, "Mission profile based reliability evaluation of capacitor banks in wind power converters," *IEEE Trans. Power Electron.,* vol. 34, no. 5, pp. 4665–4677, May 2019.

[71] J. M. Lenz, A. F. Cupertino, H. A. Pereira, D. Zhou, H. Wang, and J. R. Pinheiro, "Benchmarking of capacitor power loss calculation methods for wear-out failure prediction in PV inverters," *Microelectronics Rel.,* vol. 100/101, Sep. 2019. Art. no. 113491.

[72] W. Rohouma, R. S. Balog, A. A. Peerzada, and M. M. Begovic, "Fault-Tolerant D-STATCOM based matrix converter," in *Proc. Int. Conf. Smart Grid Renewable Energy*, Nov. 2019, pp. 2019.

[73] P. D. T. O'Connor and A. Kleyner, *Practical Reliability Engineering*, 5th ed. Wiley, Hoboken, NJ, USA, 2012.